

# Investigation of the s-shape caused by the hole selective layer in bulk heterojunction solar cells

---

Lothar Sims<sup>1,2,a)</sup>, Ulrich Hörmann<sup>1</sup>, René Kogler<sup>3</sup>, Roland Steim<sup>4</sup>, Wolfgang Brütting<sup>1</sup> and Pavel Schilinsky<sup>2</sup>

<sup>1</sup>*University of Augsburg, Institute of Physics, Universitätsstr. 1, 86135 Augsburg, Germany*

<sup>2</sup>*Belectric OPV GmbH, Landgrabenstr. 94, 90443 Nürnberg, Germany*

<sup>3</sup>*Konarka Technologies GmbH, Landgrabenstr. 94, 90443 Nürnberg, Germany*

<sup>4</sup>*Laboratory for Functional Polymers, Empa Swiss Federal Laboratories for Materials Science and Technology, Überlandstr. 129, 8600 Dübendorf, Switzerland*

During the operation period of an organic solar cell different failure mechanisms can occur which limit the lifetime of the device. Among these failure mechanisms the formation of an s-shape, where the current density-voltage curve bends towards the origin in the 4<sup>th</sup> quadrant, plays an important role. We investigated the origin of the s-shape caused by the hole-selective layer using a model system and compared experimental data with numerical simulations. As model system inverted bulk heterojunction solar cells with poly(3-hexylthiophene-2,5-diyl):[6,6]-phenyl C<sub>61</sub> butyric acid methyl ester (P3HT:PCBM) as active material and N,N'-bis(3-methylphenyl)-N,N'-bis(phenyl)-benzidine (TPD) as the hole selective layer co-evaporated with Dipyrrazino[2,3-f:2',3'-h]quinoxaline-2,3,6,7,10,11-hexacarbonitrile (HATCN) were used. The crystallization of TPD due to its low glass

---

<sup>a)</sup> Author to whom correspondence should be addressed. Electronic mail: lothar.sims@physik.uni-augsburg.de

transition temperature allows investigating the impact of work function and mobility of the hole selective layer on device performance and thus s-shape independently of each other. While the work function has an influence on the open circuit voltage, the mobility influences the s-shape and the open circuit voltage. Using input parameters derived from the measured mobilities the observed current density-voltage curves were simulated using the program PC1D which solves the fully coupled nonlinear differential equations for electrons and holes. The results show that an accumulation of holes near the hole-selective/active layer interface can be responsible for the observed s-shape.

## I. INTRODUCTION

Within the last decade intensive research to increase the efficiency of organic solar cells (OSCs) has been performed.<sup>1,2,3,4</sup> Recently, efficiencies have surmounted the psychologically important barrier of 10 % for cells fabricated in laboratory and now reach up to 12 %.<sup>5,6</sup> As a next step for commercialization it is important to transfer these efficiencies from laboratory to production. Another important aspect, which recently has received increased attention, is the stability of OSCs. Besides efficiency and cost, lifetime is the third major point which is essential for the success of organic photovoltaics. In the present work we investigate inverted OSCs with poly(3-hexylthiophene-2,5-diyl):[6,6]-phenyl C<sub>61</sub> butyric acid methyl ester (P3HT:PCBM) as active material and N,N'-bis(3-methylphenyl)-N,N'-bis(phenyl)-benzidine (TPD) as hole-selective layer (HSL) (Figure 1a). A relatively small energy barrier (<= 0.3 eV) separates the highest occupied molecular orbital (HOMO) of TPD from that of the donor polymer P3HT (Figure 1b).<sup>7,8,9</sup> The lowest unoccupied molecular orbitals (LUMOs), in

contrast, are separated by a large barrier of 1 eV.<sup>8</sup> TPD should thus be an adequate material as HSL.

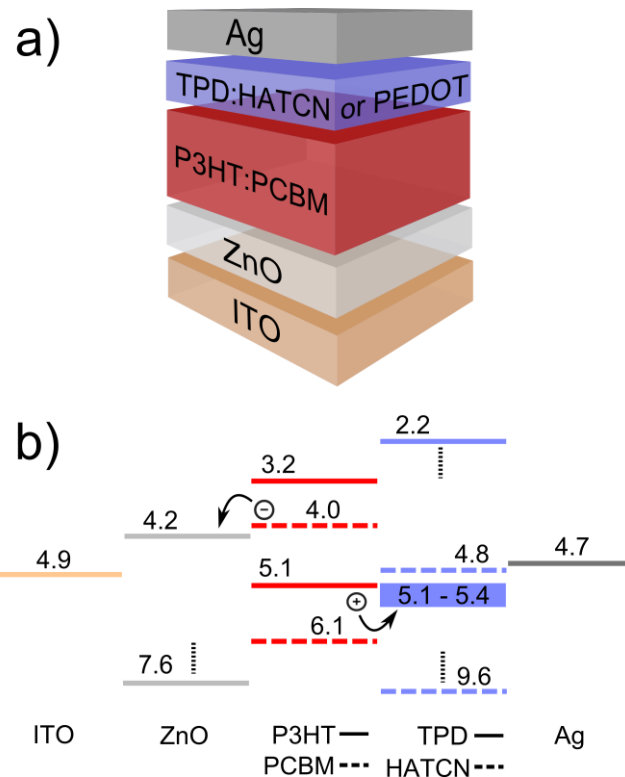


**Figure 1 - a)** Layer sequence of the investigated OSCs. **b)** Energy levels of ITO and Ag were obtained by KP-measurements, the other values are from literature.<sup>7,8, 10,11,12</sup> Vertical dashed lines indicate discontinuities.

Nevertheless, the current-voltage (*JV*) curves of cells comprising pure TPD exhibit a so-called s-shape. This term denotes a characteristic shape of the *JV*-curve, showing an inflection point around  $V_{oc}$  and thus a reduced fill factor (FF), often even below 25 % (Figure 2). This characteristic shape commonly appears during degradation of OSCs and thus plays an important role for their lifetime. By co-evaporation of various amounts of Dipyrzano[2,3-f:2',3'-h]quinoxaline-2,3,6,7,10,11-hexacarbonitrile (HATCN) together with TPD we establish a model system where the strength of the s-shape can be controlled (Figure 2).

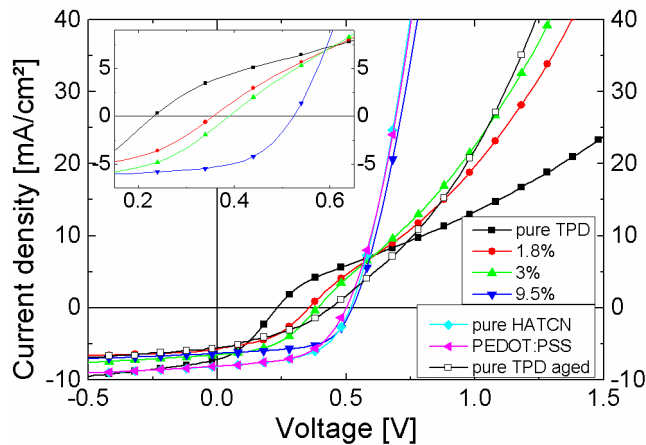


**Figure 2 - JV-curves of samples with pristine pure TPD, TPD:HATCN (1.8, 3.0 and 9.5 %), pure HATCN and PEDOT:PSS as HSL. The curve with open squares shows the sample with pure TPD after storage of 500 h in a nitrogen atmosphere at room temperature. Inset: magnification around  $V_{oc}$ .**

In literature different reasons for s-shapes have been proposed:

By simulation Wagenpfahl et al. found that a reduced surface recombination velocity at the HSL/active layer interface hinders efficient hole extraction.<sup>13</sup> Accumulated holes then change the slope of the energy levels and thus the electric field which finally leads to an s-shape. Castro et al. investigated interpenetrating bilayer OSCs.<sup>14</sup> They suggested that isolated aluminum nanoclusters in the active layer close to the interface are formed upon evaporation. These nanoclusters then act as trap states which are filled with charges, modifying the electric potential drop inside the device. They further concluded that the main effect of buffer layers such as bathocuproine (BCP) is to protect the active layer from metal diffusion. However, Wang et al. showed that increasing the thickness of the BCP layer in bilayer devices can also lead to an s-shape.<sup>15</sup> They argued that thick BCP layers consist of two regions, an unaffected and a metal permeated one. While the metal permeation causes favorable hopping sites for electrons the unaffected BCP forms a barrier for electrons. Thus, charge accumulation inside

the active layer takes place which then causes the observed s-shape. Wagner et al. showed that trap states in the active layer cannot only be induced by top electrode diffusion but also caused by impurities in the active material itself and confirmed that injection barriers may cause s-shapes in the case of planar heterojunctions.<sup>16</sup> Tress et al. found that in the case of both, bilayer and blend structures, extraction barriers, i.e. a mismatch of the HOMOs of donor and HSL can be responsible for the s-shape.<sup>17</sup>

With the help of simulations of *JV*-curves we show that an insufficient hole mobility ( $\mu$ ) of the HSL leads to an accumulation of holes near the HSL/active layer interface. This accumulation can be used as one explanation for the observed s-shape.

## II. EXPERIMENTAL

Inverted OSCs were prepared on flexible substrates by doctor blading and evaporation. As first step an 80 nm thick layer of ZnO nanoparticles was coated from solution on a PET substrate with ITO as transparent electrode.<sup>18</sup> The ZnO layer was then annealed at 140 °C for 5 minutes on a hot plate in ambient air. Subsequently, 300 nm of P3HT (Merck) mixed with [6,6]-phenyl C<sub>61</sub> butyric acid methyl ester (PCBM) (Solenne) in the ratio 1:0.8 by weight were doctor bladed on top of the ZnO layer. For reference cells a layer of Poly(3,4-ethylenedioxythiophene)-poly(styrenesulfonate) (PEDOT:PSS, Clevios PH) was bladed on the active layer. After doctor blading in ambient air, the cells were transferred into a nitrogen filled glove box and annealed again on a hot plate at 140 °C for 5 minutes. After this step the cells were kept under nitrogen atmosphere throughout the rest of the experiment. Pure TPD, TPD:HATCN or pure HATCN were evaporated (14 nm) at 1x10<sup>-6</sup> mbar. The ratio of HATCN was varied between 1 and 10 % relative to the TPD amount with an estimated absolute error of about 0.5%. The cells were finished with a 150 nm thick layer of evaporated silver as top electrode. *JV*-curves were measured under simulated AM1.5G illumination with an intensity

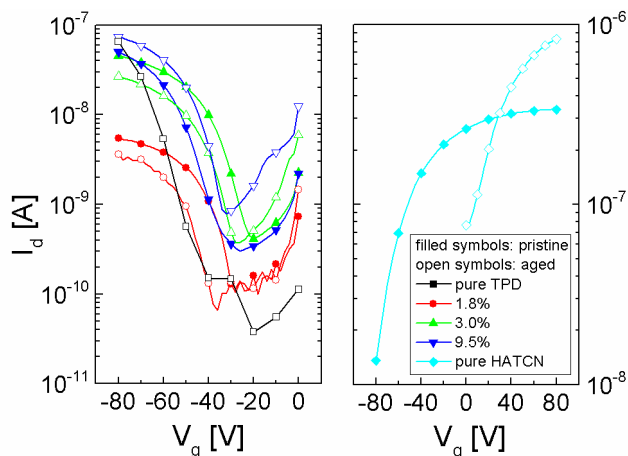
of 100 mW/cm<sup>2</sup>. For mobility measurements organic field effect transistors (OFETs) were prepared using a p-doped silicon wafer covered with a 230 nm thick SiO<sub>2</sub> layer and gold meander structures with different channel lengths of 5, 10, 15 and 20 μm. Work functions ( $\Phi$ ) were determined by Kelvin-Probe (*KP*) measurements using ITO covered PET as substrate and highly oriented graphite with a  $\Phi$  of 4.65 eV as reference. The OFETs as well as the devices for KP-measurements were evaporated simultaneously with the OSCs.

### III. RESULTS

Current-voltage characteristics of solar cell devices under AM 1.5G illumination are presented in Figure 2. Devices comprising pure TPD, TPD:HATCN mixtures and pure HATCN as hole-selective layers are shown, a PEDOT:PSS cell is displayed for reference. These curves exhibit differently pronounced s-shapes. A loss in injection current is accompanied by a loss in open circuit voltage ( $V_{oc}$ ). Depending on the amount of HATCN co-evaporated with TPD the characteristic of the s-shape changes. For pure TPD the s-shape is most pronounced, with increasing HATCN content the s-shape starts to vanish and  $V_{oc}$  and  $FF$  increase. Interestingly, the *JV*-curve of pure HATCN has a similar shape as the one of PEDOT:PSS. Looking at the energy levels of HATCN (Figure 1b) this is rather unexpected since the HOMO of HATCN differs strongly from that of P3HT (-9.6 and -5.1eV, respectively).<sup>19,10</sup>

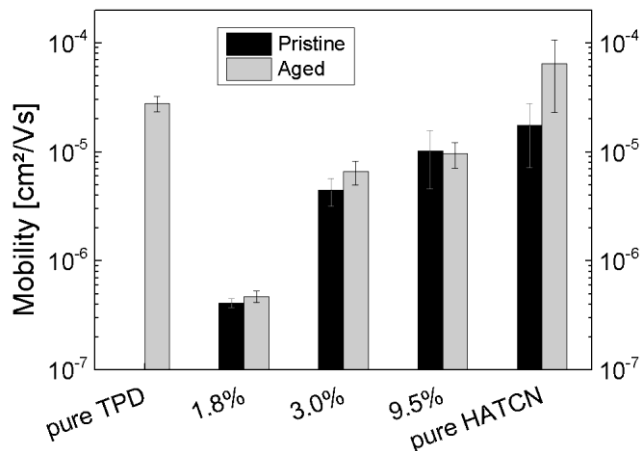
In order to elucidate the origin of the differently pronounced s-shapes, we investigated the transport properties and work functions of the HSL variations. First, measurements of  $\mu$  on OFETs with pure TPD and TPD:HATCN will be described showing varying  $\mu$  with varying HATCN content. Additionally, the impact of crystallization of the TPD layer on  $\mu$  will be discussed. Thereafter, *KP*-measurements will be shown indicating a variation of  $\Phi$  with different HATCN doping.

Figure 3 presents OFET transfer characteristics of the different variations. In the case of freshly prepared, pure TPD layers no drain current ( $I_d$ ) is visible even at high negative gate voltages ( $V_g$ ). Consequently, the mobility could not be determined for this device and is assumed to be below our measurement limit. In literature, a broad range of mobilities for pure TPD is found, strongly depending on the measurement technique.<sup>20,21</sup> Yet, a field effect mobility of  $1.6 \times 10^{-6}$  cm<sup>2</sup>/Vs is reported.<sup>22</sup> Assuming our  $\mu$  of the lowest HATCN concentration as a lower measurement limit and considering the general trend of increasing  $\mu$  with increasing HATCN content, we roughly estimate the mobility of the pristine TPD film to be around  $0.5-1 \times 10^{-7}$  cm<sup>2</sup>/Vs. As soon as the TPD film becomes doped by 1.8 % of HATCN, a hole current becomes visible and a threshold voltage ( $V_t$ ) of around -35 V as well as a mobility of  $4.1 \times 10^{-7}$  cm<sup>2</sup>/Vs can be determined. If the HATCN concentration is increased to 3 % and 9.5 %, the hole mobility increases to  $4.4 \times 10^{-6}$  cm<sup>2</sup>/Vs and  $1 \times 10^{-5}$  cm<sup>2</sup>/Vs, respectively. Note that the latter devices show ambipolar behavior, which indicates that electrons are present in the transistor above certain gate voltages.



**Figure 3 – Transfer characteristics at a drain voltage of -20V for curves on the left and +20V for the curve on the right. Before storage of 500 h under nitrogen at room temperature the current of the pure TPD sample was below the measurement sensitivity.**

In particular, the pure HATCN FET solely shows n-type behavior and an *electron* mobility of  $\mu_e = 1.8 \times 10^{-5} \text{ cm}^2/\text{Vs}$  can be derived in this case. For pure TPD a hole current becomes clearly visible after storing the device in nitrogen atmosphere at room temperature for approx. 500 h. Crystallization changes the TPD layer from an amorphous to a more ordered film. This is accompanied by a visual change from a transparent to a matte appearance and is ascribed to the low glass transition temperature of TPD of around 60 °C.<sup>23</sup> Thus, a hole mobility of  $2.8 \times 10^{-5} \text{ cm}^2/\text{Vs}$  and a threshold voltage of around -50 V can now be derived for aged TPD. In case of the TPD:HATCN mixtures no change, neither visually nor in the JV-curves, was observed and no change of  $\mu$  was measured. This can be explained by higher thermal stability of TPD in combination with HATCN.<sup>24</sup> The carrier mobilities of all pristine and aged devices are shown in Figure 4.



**Figure 4** -  $\mu$  of pure TPD, TPD:HATCN (1.8, 3.0 and 9.5 %) and pure HATCN. Black: pristine samples; Gray: after 500 h under nitrogen at room temperature. The values are average values of  $\mu$  calculated from the output and transfer characteristic of OFETs. For pure TPD directly after preparation  $\mu$  is too small for measurement, thus, only the value after 500 h storage is given.

Besides an increase of  $\mu$  with increasing HATCN content also an increase of  $\Phi$  was measured (Figure 5). Note that the work function of the pure TPD layer remains at around 4.6 eV, virtually unaffected by the crystallization. The fact that TPD aging changes the mobility but not the work function will be helpful in order to separate mobility and energy barriers as possible causes of the s-shape.

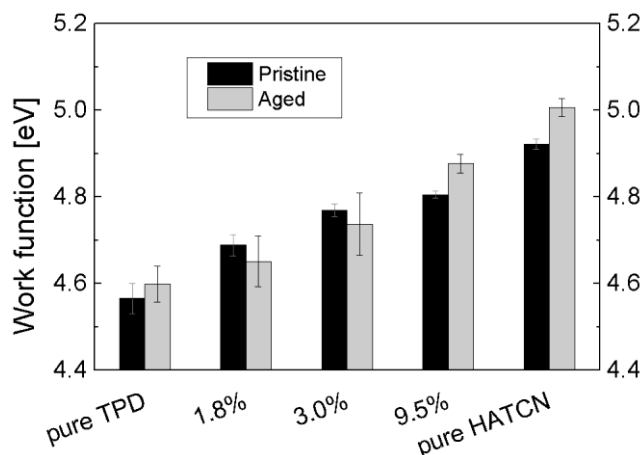


**Figure 5 -  $\Phi$  of pure TPD, TPD:HATCN (1.8, 3.0 and 9.5 %) and pure HATCN on ITO. Black: pristine samples; Gray: after 500 h under nitrogen at room temperature.**

#### IV. SIMULATION

In order to reveal the detailed impact of  $\mu$  of the HSL on the  $JV$ -curve and to confirm the experimental results we performed numerical simulations of the  $JV$ -curves with PC1D. The program was developed by P. A. Basore and D. A. Clugston from the University of New South Wales and originally used for the simulation of inorganic semiconductors. It was shown that the program also applies, at least with some limitations, to organic bulk heterojunction solar cells.<sup>25,26,27</sup> The program solves the fully coupled nonlinear differential equations, i.e. the transport, continuity and Poisson equations for electrons and holes. The

blend of P3HT:PCBM is simulated as one effective semiconductor material using the HOMO of P3HT as valence and the LUMO of PCBM as conduction band. The band gap of P3HT is used to simulate the intrinsic absorption of photons. The electron selective layer is assumed to have an electron affinity of 4.2 eV, which corresponds to the conduction band of ZnO, while the ionization potential of the HSL is 5.4 eV, which corresponds to the HOMO of TPD. Besides *JV*-curves, the program is also able to simulate spatially resolved charge carrier densities and electric fields. Figure 6 shows the simulated *JV*-curves. The only parameter varied for the curves of pure TPD, 1.8 %, 3.0 % and 9.5 % HATCN doped TPD was  $\mu$  of the holes, starting with  $1 \times 10^{-6}$  cm<sup>2</sup>/Vs for pure TPD (Table I). This value, instead of the experimental value in the range of  $10^{-7}$  cm<sup>2</sup>/Vs, was chosen because PC1D does not support a lower  $\mu$ . Thus, the simulation is a qualitative and not quantitative analysis. However, the increase of  $\mu$  in the simulation covers the same range as the results for  $\mu$  obtained by OFET-measurements and accounts for the increasing HATCN concentration in the layer.

**Table I – Mobility  $\mu$  as measured and as used for the simulated *JV*-curves shown in Figure 6. Since  $1 \times 10^{-6}$  cm<sup>2</sup>/Vs is the lower limit of PC1D, this value was chosen for the pure TPD film. The other values were chosen in order to cover a span similar to the measurement.<sup>28</sup>**

| Sample      | $\mu_h$ [cm <sup>2</sup> /Vs]<br>(measurement) | $\mu_h$ [cm <sup>2</sup> /Vs]<br>(simulation) |
|-------------|--|---|
| pure TPD    | $0.5\text{--}1.0 \times 10^{-7}$ (estimated)   | $1 \times 10^{-6}$                            |
| 1.8 % HATCN | $4.1 \times 10^{-7}$                           | $6 \times 10^{-6}$                            |
| 3.0 % HATCN | $4.4 \times 10^{-6}$                           | $1 \times 10^{-5}$                            |
| 9.5 % HATCN | $1.0 \times 10^{-5}$                           | $5 \times 10^{-4}$                            |

A two and a half orders of magnitude increase of  $\mu$  fully restores the  $JV$ -curve (Figure 6).

This is in agreement with the measurements described above (Figure 2). In addition, the simulation shows that a change of  $\mu$  alone can also lead to a change in  $V_{oc}$  (inset Figure 6).

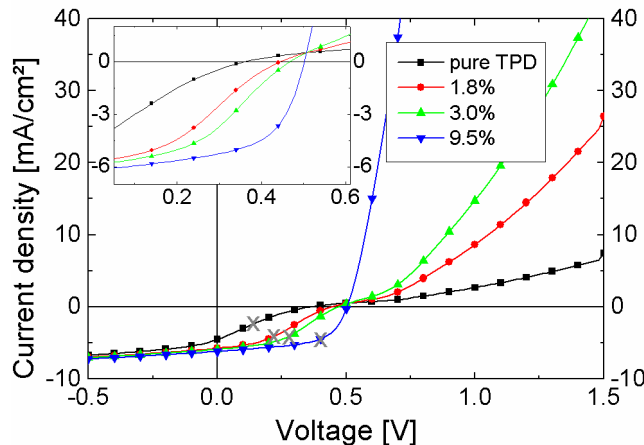


**Figure 6 - Simulated  $JV$ -curves.** Besides  $\mu$  all other parameters were kept constant. Pure TPD has the lowest and 9.5 % the highest  $\mu$  (Table I). The crosses show the maximum power point. Inset: magnification around  $V_{oc}$ .

Figure 7 shows the charge carrier densities of electrons and holes at maximum power point voltage applied. An increased hole density in the HSL and a peak in the active layer near the interface for low mobilities is observed. The highest concentration in the HSL can be observed for pure TPD. In this case also the peak in the active layer reaches the highest value. Near the electrode the concentration starts to decrease. This shows that more holes are reaching the HSL/active layer interface than can be transferred by the HSL to the electrode. As a result, the electric field inside the active layer is reduced (inset Figure 7). Increasing  $\mu$  leads to a decrease of the concentration of holes in the HSL and the peak in the active layer, which in turn increases the electric field. For the highest value of  $\mu$  the hole density in the HSL amounts only to a fraction of the density received for pure TPD. Further, the

concentration in the HSL is constant also near the electrode and there is no peak at the HSL/active layer interface anymore. Hole transfer rate and transport to the electrode start to balance.

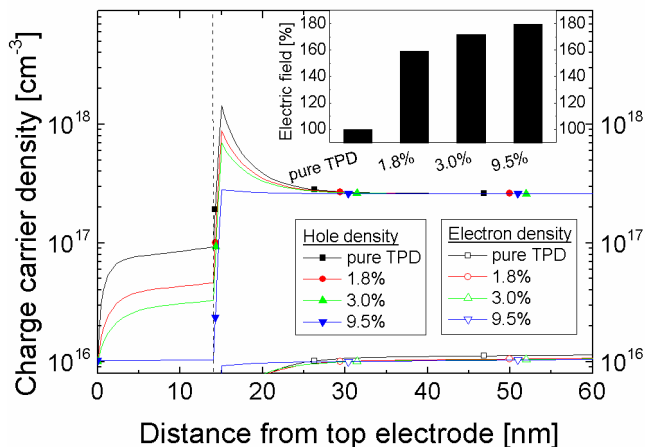


**Figure 7 - Charge carrier density of holes and electrons within OSCs for pure TPD and different TPD:HATCN ratios (1.8, 3.0, 9.5 %) as obtained from simulation with PC1D at maximum power point conditions. Only  $\mu$  was changed (Table I). The dashed line at 14 nm indicates the interface of HSL and active layer. Inset: electric field within the active layer, pure TPD = 100%.**

## V. DISCUSSION

### A. Interface energetics and charge transport in the hole selective layer

A brief introduction of the transport and injection mechanism at the HSL is given before discussing the correlation of the s-shape and the hole mobility of the HSL.

In general, the energy difference between  $\Phi$  of the metal contact and the HOMO of the HSL is regarded as the hole injection barrier (HIB). The effective electrode work function ( $\Phi_{eff}$ ) shown in Figure 5 increases with increasing HATCN content. Assuming that the HOMO level of TPD remains energetically unchanged, this implies a reduction of the HIB with larger

amounts of HATCN. Note that even though  $\Phi$  was measured on an ITO substrate the effective work functions of the corresponding Ag/HSL electrodes are expected to be similar. The difference between  $\Phi$  of the clean substrate (4.9 eV for ITO) and  $\Phi_{eff}$  with the HSL on top can be explained by contribution of two counter-acting mechanisms, namely the push-back effect and Fermi level pinning. The so-called push-back effect will lead to a reduced  $\Phi$  by reducing (“pushing back”) the electron-density “leaking” from the metal into vacuum. In the case of pure TPD  $\Phi$  is reduced to 4.6 eV. This shift is in agreement with values of 0.2 – 0.4 eV reported in literature and attributed to the change of the interface dipole by the push-back effect.<sup>7,29,30</sup> The effect has also been reported to reduce  $\Phi$  of metal substrates, including Ag and Au, whereas the strength of the shift depends on the pretreatment of the substrate.<sup>7,31,32</sup> On the other hand, as soon as HATCN is introduced to the film, unoccupied states from the HATCN LUMO are present (Figure 1b). This enables charge transfer from the metal to the HSL and an interface dipole is formed which counteracts the push-back effect and increases  $\Phi$ . As larger amounts of HATCN are present, this effect becomes stronger and results in the observed gradual increase of  $\Phi_{eff}$ . In the case of pure HATCN this charge transfer leads to Fermi level pinning at the negative polaron level of HATCN and eliminates the HIB.<sup>30,32,33</sup>

As mentioned above the presence of electrons in the HATCN LUMO is visible in the ambipolar and n-type behavior of the OFETs containing HATCN even at negative gate voltages and is crucial for hole extraction when pure HATCN is applied as HSL in solar cells. Electrons stemming from the Ag electrode are present in the HATCN LUMO and recombine with holes coming from the P3HT layer. This is essentially equivalent to holes being extracted and similar to the working mechanism of MoO<sub>3</sub> whose conduction and valence band are in a similar range as the LUMO and HOMO of HATCN.<sup>34</sup> Consequently, in the case of hole injection under forward bias electrons are extracted from the P3HT HOMO via the

HATCN LUMO. Consequently, the electron mobility of HATCN has to be regarded as the relevant mobility of the “hole-selective” layer, if pure HATCN is used.

The effect of increasing  $\mu$  with increasing HATCN content in the TPD:HATCN layer can be explained in terms of the multiple-trapping-and-release model.<sup>35</sup> A possible consequence of co-evaporation of HATCN with TPD might be that low lying states in the tail of the Gaussian distribution are filled up with charges and are thus no more available for other charges. The probability for charges moving through TPD of being trapped is reduced which in turn leads to an increased  $\mu$ .<sup>36</sup> Furthermore, HATCN can serve as additional transport channel once the concentration is high enough.

## B. Factors affecting the open circuit voltage

The maximum possible  $V_{oc}$  of a donor-acceptor combination is determined by the difference of  $\text{HOMO}_{\text{donor}}$  and  $\text{LUMO}_{\text{acceptor}}$  and is usually reduced by about 0.5 eV at room temperature because of the charge transfer state, Coulomb interaction and recombination.<sup>19,37,38,39,40</sup>

Additionally,  $V_{oc}$  is influenced by the energy levels of the adjacent layers and cannot exceed the built-in potential  $V_{bi}$  in BHJ cells.<sup>41,42,43,44,45</sup>

Looking at the trend of the open circuit voltage of the pristine devices in Figure 2 one can conclude that  $V_{oc}$  increases with increasing HATCN content and saturates for a concentration of 9.5 %. This correlates with the observed increase of the  $\Phi_{eff}$  of the electrode, which in turn is expected to raise  $V_{bi}$ . Note that if the electron affinity of ZnO is regarded as the relevant energy level for electron extraction,  $V_{bi}$  for the 9.5 % HATCN cell would equal 0.6 V and thus match the expected possible  $V_{oc}$  value for the P3HT:PCBM junction at room temperature. This observation suggests that an effective work function of at least 4.8 eV of the electrode on the hole selective side is necessary in order to reach full  $V_{oc}$  for this type of solar cell.

We would like to point out that the work function alone is not responsible for the drastically reduced  $V_{oc}$  of the pristine cells. Analysis of aged, pure TPD device reveals that  $V_{oc}$  roughly doubles as the mobility is increased while  $\Phi$  remains unchanged. In particular  $\Phi$  is still lower for this device than for the TPD:HATCN mixtures. The  $V_{oc}$ , however, is larger than for the 1.8 % and 3 % HATCN cells and so is the mobility. Thus, it is important to notice that an insufficient mobility can also reduce  $V_{oc}$ . Such a reduction by the hole mobility is also seen in the simulation (inset Figure 6) even though it is less drastic. This can be explained by the input mobility of  $1 \times 10^{-6} \text{ cm}^2/\text{Vs}$  which is about one order of magnitude larger than in the real device. The qualitative charge density profile in Figure 7 shows that a low hole mobility gives rise to charge accumulation at the HSL/active layer interface. This accumulated hole density causes a large concentration gradient, which favors a diffusion current. This leads to additional recombination current and thus results in a reduced open circuit voltage. We conclude that a mobility below  $1 \times 10^{-5} \text{ cm}^2/\text{Vs}$  in the HSL is detrimental for the open circuit voltage of the solar cell.

### C. Origin of the s-shape

The increase of  $V_{oc}$  with increasing HATCN content seen for the devices in Figure 2 is associated with a change of the shape of the  $JV$ -curve. While a pronounced s-shape is present in the pristine, pure TPD device, introducing HATCN to the HSL gradually reduces this effect. As mentioned above energetic barriers have previously been found to be responsible for s-shaped  $JV$ -curves.<sup>16,17</sup> In our case, we also see a reduction of the HIB with increasing HATCN concentration. However, this is accompanied by a strong increase in mobility. A comparison of pristine and aged TPD shows that the s-shape is drastically reduced by the increased mobility of the crystalline TPD film, even though the HIB can be assumed to stay constant. This correlation between s-shape and  $\mu$  rather than with the HIB is a clear hint that in our case the mobility of the HSL layer is responsible for the slope of the  $JV$ -curve and thus

the s-shape. This was discussed similarly in<sup>25</sup>, where conductivity of interface materials was assumed as origin of s-shapes and is clearly reflected in the simulated JV-curves shown in Figure 6. Here, an increase of  $\mu$  by a factor of  $10^{2.5}$ , as measured in experiment, clearly reduces the s-shape and leads to a strongly increased injection current. Again, as the lower mobility limit for simulation is  $1 \times 10^{-6} \text{ cm}^2/\text{Vs}$  a quantitative comparison of measured (Figure 2) and simulated (Figure 6) JV-curves is not possible. Baring in mind that  $\mu$  is the only parameter varied in the simulation we conclude that insufficient mobility in the HSL can solely be responsible for s-shaped JV-curves.

As mentioned before, an elevated hole density occurs in the HSL and at the HSL/active layer interface which becomes larger for lower mobilities (Figure 7). This accumulation leads to a space charge region and thus a barrier for holes at the HSL/active layer interface and reduces the electric field within the active layer (inset Figure 7) which then becomes visible as the s-shape.

## VI. CONCLUSION

Organic solar cells with different hole-selective layers consisting of evaporated TPD, TPD:HATCN mixtures and HATCN were produced. The mobilities of these hole-selective layers reached from around  $10^{-7}$  to over  $10^{-5} \text{ cm}^2/\text{Vs}$ . We could show that pure HATCN can serve as hole selective layer even though charge transport is achieved by electrons. By controlling the mobility of the hole selective layer it was possible to influence the strength of the s-shape. The crystallization of the pure TPD film could be used to separate the influence of mobility and hole injection barrier on the s-shape. The morphological changes increased the mobility but did not affect the effective work function. The increase in mobility was accompanied by a drastic gain in  $V_{oc}$  and decrease of the s-shape. This is in accordance with the increased  $V_{oc}$  and reduced s-shape found for increasing HATCN concentrations in the

hole selective layer. Further, numerical simulations confirmed that an insufficient hole mobility of the hole selective layer induces s-shaped *JV*-characteristics. Consequently, particular attention has to be paid to the mobility of the hole selective layer to reach optimum and long-life performance of organic solar cells.

## ACKNOWLEDGEMENTS

L.S. thanks Hans-Joachim Egelhaaf for fruitful discussions.

## REFERENCES

- <sup>1</sup> C.J. Brabec, S.E. Shaheen, C. Winder, N.S. Sariciftci, and P. Denk, *Appl. Phys. Lett.* **80**, 1288 (2002).
- <sup>2</sup> W. Ma, C. Yang, X. Gong, K. Lee, and A.J. Heeger, *Adv. Func. Mater.* **15**, 1617 (2005).
- <sup>3</sup> G. Zhao, Y. He, and Y. Li, *Adv. Mater.* **22**, 4355 (2010).
- <sup>4</sup> Y. Liang, Z. Xu, J. Xia, S.-T. Tsai, Y. Wu, G. Li, C. Ray, and L. Yu, *Adv. Mater.* **22**, E135 (2010).
- <sup>5</sup> M.A. Green, K. Emery, Y. Hishikawa, W. Warta, and E.D. Dunlop, *Prog. Photovolt: Res. Appl.* **20**, 12 (2012).
- <sup>6</sup> [http://www.heliatek.com/newscenter/latest\\_news/neuer-weltrekord-fur-organische-solarzellen-heliatek-behauptet-sich-mi.-12-zelleffizienz-als-technologiefuehrer/?lang=en](http://www.heliatek.com/newscenter/latest_news/neuer-weltrekord-fur-organische-solarzellen-heliatek-behauptet-sich-mi.-12-zelleffizienz-als-technologiefuehrer/?lang=en)  
Heliatek GmbH, (2013).
- <sup>7</sup> L. Chkoda, C. Heske, M. Sokolowski, E. Umbach, F. Steuber, J. Staudigel, M. Stössel, and J. Simmerer, *Synthetic Met.* **111-112**, 315 (2000).
- <sup>8</sup> J. Yang and K.C. Gordon, *Chem. Phys. Lett.* **375**, 649 (2003).
- <sup>9</sup> J.Y. Kim, K. Lee, N.E. Coates, D. Moses, T.-Q. Nguyen, M. Dante, and A.J. Heeger, *Science* **317**, 222 (2007).

<sup>10</sup> C. Falkenberg, S. Olthof, R. Rieger, M. Baumgarten, K. Müllen, K. Leo, and M. Riede, Sol. Energy Mater. Sol. Cells **95**, 927 (2011).

<sup>11</sup> M.O. Reese, M.S. White, G. Rumbles, D.S. Ginley, and S.E. Shaheen, Appl. Phys. Lett. **92**, 053307 (2008).

<sup>12</sup> I. Park, Y. Lim, S. Noh, D. Lee, M. Meister, J.J. Amsden, F. Laquai, C. Lee, and D.Y. Yoon, Org. Electron. **12**, 424 (2011).

<sup>13</sup> A. Wagenpfahl, D. Rauh, M. Binder, C. Deibel, and V. Dyakonov, Phys. Rev. B **82**, 115306 (2010).

<sup>14</sup> F.A. de Castro, J. Heier, F. Nuesch, and R. Hany, IEEE J. Sel. Top. Quant. **16**, 1690 (2010).

<sup>15</sup> J.C. Wang, X.C. Ren, S.Q. Shi, C.W. Leung, and P.K.L. Chan, Org. Electron. **12**, 880 (2011).

<sup>16</sup> J. Wagner, M. Gruber, A. Wilke, Y. Tanaka, K. Topczak, A. Steindamm, U. Hörmann, A. Opitz, Y. Nakayama, H. Ishii, J. Pflaum, N. Koch, and W. Brüttig, J. Appl. Phys. **111**, 054509 (2012).

<sup>17</sup> W. Tress, K. Leo, and M. Riede, Adv. Funct. Mater. **21**, 2140 (2011).

<sup>18</sup> S.K. Hau, H.-L. Yip, N.S. Baek, J. Zou, K. O'Malley, and A.K.-Y. Jen, Appl. Phys. Lett. **92**, 253301 (2008).

<sup>19</sup> D. Veldman, S.C.J. Meskers, and R.A.J. Janssen, Adv. Funct. Mater. **19**, 1939 (2009).

<sup>20</sup> A. Kuwahara, S. Naka, H. Okada, and H. Onnagawa, Appl. Phys. Lett. **89**, 132106 (2006).

<sup>21</sup> M. Aonuma, T. Oyamada, H. Sasabe, T. Miki, and C. Adachi, Appl. Phys. Lett. **90**, 183503 (2007).

<sup>22</sup> K. Kudo, M. Iwamoto, K. Kaneto, and S. Mashiko, *Nanotechnology and Nano-Interface Controlled Electronic Devices* (Elsevier Science B.V., Amsterdam, 2003) p.172.

<sup>23</sup> K. Naito and A. Miura, J. Phys. Chem. **97**, 6240 (1993).

<sup>24</sup> T. Krieg, A. Petr, G. Barkleit, and L. Dunsch, *Appl. Phys. Lett.* **74**, 3639 (1999).

<sup>25</sup> R. Steim, *The Impact of Interfaces on the Performance of Organic Photovoltaic Cells* (KIT Scientific Publishing, Karlsruhe, 2010) p.15.

<sup>26</sup> A. Seemann, T. Sauermann, C. Lungenschmied, O. Armbruster, S. Bauer, H.-J. Egelhaaf, and J. Hauch, *Sol. Energy* **85**, 1238 (2011).

<sup>27</sup> P. Schilinsky, Ph.D. thesis, University of Oldenburg, 2005.

<sup>28</sup> See supplementary material at [URL] for the full set of parameters used in the simulation.

<sup>29</sup> H. Peisert, T. Schwieger, M. Knupfer, M.S. Golden, and J. Fink, *J. Appl. Phys.* **88**, 1535 (2000).

<sup>30</sup> H.M.S.B. Bröker, Ph.D. thesis, Humboldt University of Berlin, 2010.

<sup>31</sup> H. Ishii, N. Hayashi, E. Ito, Y. Washizu, K. Sugi, Y. Kimura, M. Niwano, Y. Ouchi, and K. Seki, *Phys. Status Solidi A* **201**, 1075 (2004).

<sup>32</sup> S. Braun, W.R. Salaneck, and M. Fahlman, *Adv. Mater.* **21**, 1450 (2009).

<sup>33</sup> J. Niederhausen, P. Amsalem, J. Frisch, A. Wilke, A. Vollmer, R. Rieger, K. Müllen, J.P. Rabe, and N. Koch, *Phys. Rev. B* **84**, 165302 (2011).

<sup>34</sup> J. Meyer and A. Kahn, *Journal of Photonics for Energy* **1**, 011109 (2011).

<sup>35</sup> R. Schmeichel, *J. Appl. Phys.* **93**, 4653 (2003).

<sup>36</sup> S. Olthof, S. Mehraeen, S.K. Mohapatra, S. Barlow, V. Coropceanu, J.-L. Brédas, S.R. Marder, and A. Kahn, *Phys. Rev. Lett.* **109**, (2012).

<sup>37</sup> U. Hörmann, J. Wagner, M. Gruber, A. Opitz, and W. Brüttig, *Phys. Status Solidi RRL* **5**, 241 (2011).

<sup>38</sup> M.C. Scharber, D. Mühlbacher, M. Koppe, P. Denk, C. Waldauf, A.J. Heeger, and C.J. Brabec, *Adv. Mater.* **18**, 789 (2006).

<sup>39</sup> A. Wilke, J. Endres, U. Hörmann, J. Niederhausen, R. Schlesinger, J. Frisch, P. Amsalem, J. Wagner, M. Gruber, A. Opitz, A. Vollmer, W. Brütting, A. Kahn, and N. Koch, *Appl. Phys. Lett.* **101**, 233301 (2012).

<sup>40</sup> M. Gruber, J. Wagner, K. Klein, U. Hörmann, A. Opitz, M. Stutzmann, and W. Brütting, *Adv. Energy Mater.* **2**, 1100 (2012).

<sup>41</sup> H. Frohne, S.E. Shaheen, C.J. Brabec, D.C. Müller, N.S. Sariciftci, and K. Müllen, *ChemPhysChem* **9**, 795 (2002).

<sup>42</sup> S.O. Jeon, K.S. Yook, B.D. Chin, Y.S. Park, and J.Y. Lee, *Sol. Energy Mater. Sol. Cells* **94**, 1389 (2010).

<sup>43</sup> V.D. Mihailescu, P.W.M. Blom, J.C. Hummelen, and M.T. Rispens, *J. Appl. Phys.* **94**, 6849 (2003).

<sup>44</sup> R. Steim, F.R. Kogler, and C.J. Brabec, *J. Mater. Chem.* **20**, 2499 (2010).

<sup>45</sup> C. Uhrich, D. Wynands, S. Olthof, M.K. Riede, K. Leo, S. Sonntag, B. Maennig, and M. Pfeiffer, *J. Appl. Phys.* **104**, 043107 (2008).